acta physica slovaca vol. 46 No. 4, 585 – 610 August 1996

NUMERICAL STUDY OF SPECTRUM AND HBT RADII FOR THREE-DIMENSIONALLY EXPANDING CYLINDRICALLY SYMMETRIC FINITE SYSTEMS[1]

T. Csörgö[†‡2], P. Lévai[‡3], B. Lörstad[¶4]

[†]*Department of Physics, Columbia University, 538 West 120th, New York, NY 10027*

[‡]*MTA KFKI RMKI, H – 1525 Budapest 114, POB 49, Hungary*

[¶]*Physics Institute, University of Lund, POB 118, S – 221 00 Lund, Sweden*

Received 23. April 1996, accepted 15 May 1996

This study is devoted to a detailed numerical testing of the analytical results obtained recently for the *M_t-scaling* of the parameters of the Bose-Einstein correlation functions. Numerical testing of analytical results for the spectrum is also performed, since the geometrical sizes are folded into the momentum distribution in the scaling limiting case. The analytical results are shown to be valid in a wider rapidity-range than thought before.

1. Introduction

Recently there has been much interest in the measurement and the calculation of the parameters of Bose-Einstein correlation functions (BECF-s) and those of the invariant momentum distributions (IMD-s) for rapidly expanding systems with flow and temperature profiles. Such systems are expected to be formed in high energy heavy ion reactions. The quality and the amount of available data improved drastically mainly due to the efforts of NA35, NA44, NA49 and WA93 collaborations at CERN [1, 2, 3, 4]. Data from the dedicated HBT experiment NA44 indicated an unexpected, scaling behavior for the parameters of the BECF-s [2]. Within the errors of this measurement, the R_{side}, R_{out} and R_{long} parameters of the BECF for $S + Pb$ 200 AGeV central reactions turned out to be equal and all were found to scale simultaneously, proportionally to $1/\sqrt{M_t}$, where M_t is the transverse mass of the identical particle pair. This scaling relation is found to be independent of the particle type at the present level of experimental precision.

This new generation of HBT data triggered a burst of activity mainly from the Budapest [5, 6, 7, 8, 9, 10], Kiev [11, 12, 13], Marburg [14, 15] and Regensburg [16,

[1] Presented at the School and Workshop on Heavy Ion Collisions, Sept. 4.-8., 1995, Bratislava

[2] E-mail address: csorgo@sgiserv.rmki.kfki.hu

[3] E-mail address: plevai@rmki.kfki.hu

[4] E-mail address: bengt@quark.lu.se

17, 18, 19] groups, aiming at interpreting the data in terms of collective, hydrodynamic behavior. The results from Los Alamos group [20] also indicate collective behavior caused by re-scattering of secondary particles in the framework called RQMD event generator. These results are also supported by simulations of re-scattering effects in a hot expanding gas of hadrons [21]. It became clear, that Bose-Einstein correlations are in general not measuring the whole geometrical sizes of big and expanding finite systems, neither in the longitudinal [22] nor in the transverse and temporal directions, since the expansion may result in strong correlations between space-time and momentum space variables not only in the longitudinal, but in the transverse and temporal directions, too, see ref.[9] and references therein for a more detailed account on this topic.

Where have all the geometrical sizes gone? One can show[6, 9], that they are disguised in the invariant momentum distribution of the bosons in case they cancel from the radius parameters of the Bose-Einstein correlation function (BECF).

We briefly review here the analytical results presented in refs.[5, 6, 7, 9, 10] which are tested in a detailed numerical analysis in the subsequent parts. The review of the analytical results mainly follows the lines of ref. [10], but the present review is more technical than that, since we discuss here also the details of the model emission function and that of the IMD. Ref. [10] is recommended for the illustration of the physical ideas, which determine the M_t dependencies of the parameters of BECF-s.

2. Wigner Function Formalism

The two-particle inclusive correlation function is defined and approximately expressed in the Wigner function formalism as

$$C(\Delta k;K) = \frac{\langle n(n-1)\rangle}{\langle n\rangle^2}\frac{N_2(\mathbf{p}_1,\mathbf{p}_2)}{N_1(\mathbf{p}_1)\,N_1(\mathbf{p}_2)} \simeq 1+\frac{|\,\tilde S(\Delta k,K)\,|^2}{|\,\tilde S(0,K)\,|^2}. \qquad (1)$$

In the above line, the Wigner-function formalism[23, 24, 25] is utilized assuming fully chaotic (thermalized) particle emission. The covariant Wigner-transform of the source density matrix, $S(x,p)$, is a quantum-mechanical analogue of the classical robability that a boson is produced at a given $x^\mu=(t,\mathbf{r})=(t,r_x,r_y,r_z)$ with $p^\mu=(E,\mathbf{p})=(E,p_x,p_y,p_z)$. The auxiliary quantity $\tilde S(\Delta k,K)=\int d^4x S(x,K)\exp(i\Delta k\cdot x)$ appears in the definition of the BECF, with $\Delta k=p_1-p_2$ and $K=(p_1+p_2)/2$. The single- and two-particle inclusive momentum distributions (IMD-s) are given by

$$N_1(\mathbf{p})=\frac{E}{\sigma_{tot}}\frac{d\sigma}{d\mathbf{p}}=\tilde S(\Delta k=0,p), \quad \text{and} \quad N_2(\mathbf{p_1},\mathbf{p_2})=\frac{E_1E_2}{\sigma_{tot}}\frac{d\sigma}{d\mathbf{p}_1\,d\mathbf{p}_2}, \qquad (2)$$

where σ_{tot} is the total inelastic cross-section. Note that in this work we utilize the following normalization of the emission function[7]: $\int\frac{d^3\mathbf{p}}{E}d^4xS(x,p)=\langle n\rangle$.

3. Effects from Large Halo of Long-Lived Resonances

If the bosons originate from a core which is surrounded by a halo of long-lived resonances, the IMD and the BECF can be calculated in a straightforward manner. The detailed description is given in ref.[7], here we review only the basic idea.

If the emission function can be approximately divided into two parts, representing the core and the halo, $S(x;K)=S_c(x;K)+S_h(x;K)$ and if the halo is characterized by large length-scales so that $\tilde S_h(Q_{min};K)<<\tilde S_c(Q_{min};K)$ at a finite experimental resolution of $Q_{min}\geq 10$ MeV, then the IMD and the BECF reads as

$$N_1(\mathbf{p}) = N_{1,c}(\mathbf{p})+N_{1,h}(\mathbf{p}), \qquad (3)$$

$$C(\Delta k;K) = 1+\lambda_*\frac{|\,\tilde S_c(\Delta k,K)\,|^2}{|\,\tilde S_c(0,K)\,|^2}, \qquad (4)$$

where $N_{1,i}(\mathbf{p})$ stands for the IMD of the halo or core for $i=h,c$ and

$$\lambda_* = \lambda_*(K=p)=\left[\frac{N_{1,c}(\mathbf{p})}{N_1(\mathbf{p})}\right]^2. \qquad (5)$$

Thus within the core/halo picture the phenomenological λ_* parameter can be obtained in a natural manner at a given finite resolution of the relative momentum. This parameter has been introduced to the literature by Deutschmann long time ago[26]. See ref. [7] and references therein for a more detailed account on the origin of this parameter λ_*. In the core/halo picture, the effective or measured intercept parameter $\lambda(\mathbf{p})$ *can be interpreted* as the *momentum dependent* square of the ratio of the IMD of the core to the IMD of all particles emitted.

4. General Considerations and Results

We are considering jets in elementary particle reactions or high energy heavy ion reactions, which correspond to systems undergoing an approximately boost-invariant longitudinal expansion. For expansions fully invariant for longitudinal boosts, the emission function may depend only on such variables, which are invariant for longitudinal boosts. These are defined as $\tau=\sqrt{t^2-r_z^2}$, $\eta=0.5\ln[(t+z)/(t-z)]$, $m_t=\sqrt{E^2-p_z^2}$, $y=0.5\ln[(E+p_z)/(E-p_z)]$ and $r_t=\sqrt{r_x^2+r_y^2}$. For finite systems, the emission function may depend on $\eta-y_0$ too, where y_0 stands for the mid-rapidity. Approximate boost-invariance is recovered in the $|\,\eta-y_0\,|<<\Delta y$ region, where the width of the rapidity distribution is denoted by Δy. In terms of these variables the emission function can be rewritten as

$$S_c(x;K)\,d^4x = S_{c,*}(\tau,\eta,r_x,r_y)\,d\tau\,\tau_0 d\eta\,dr_x\,dr_y. \qquad (6)$$

The subscript $_*$ indicates that the functional form of the source function is changed, and it stands for a dependence on K and y_0 also.

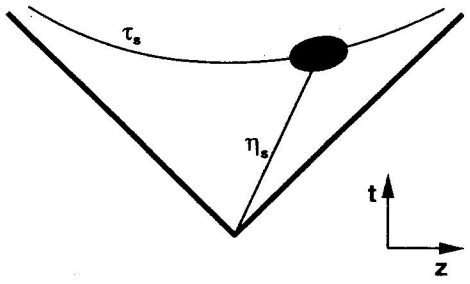

Fig. 1. Emission of particles with a given momentum is centered around τ_s and η_s for systems undergoing boost-invariant longitudinal expansion, as indicated by the shaded area.

In the standard HBT coordinate system[27], the mean and the relative momenta are $K = (K_0, K_{out}, 0, K_L)$ and $\Delta k = (Q_0, Q_{out}, Q_{side}, Q_L)$. Note that the $_{side}$ component of the mean momentum vanishes by definition[27, 9]. Since the particles are on mass-shell, we have $0 = K \cdot \Delta k = K_0 Q_0 - K_L Q_L - K_{out} Q_{out}$.

Introducing $\beta_L = K_L/K_0$ and $\beta_{out} = K_{out}/K_0$, the energy difference Q_0 can thus be expressed as

$$Q_0 = \beta_L Q_L + \beta_{out} Q_{out}. \tag{7}$$

If the emission function has such a structure that it is concentrated in a narrow region around (τ_s, η_s) in the (τ, η) plane, then one can evaluate the BECF in terms of variables τ and η by utilizing the expansion

$$\Delta k \cdot x = Q_0 t - Q_{out} r_x - Q_{side} r_y - Q_L r_z \simeq \tag{8}$$
$$Q_\tau \tau - Q_{out} r_x - Q_{side} r_y - Q_\eta \tau_s (\eta - \eta_s). \tag{9}$$

The coefficients of the τ and the $\tau_s(\eta - \eta_s)$ are new variables given by

$$Q_\tau = Q_0 \cosh[\eta_s] - Q_L \sinh[\eta_s] = (\beta_t Q_{out} + \beta_L Q_L)\cosh[\eta_s] - Q_L \sinh[\eta_s], \tag{10}$$
$$Q_\eta = Q_L \cosh[\eta_s] - Q_0 \sinh[\eta_s] = Q_L \cosh[\eta_s] - (\beta_t Q_{out} + \beta_L Q_L)\sinh[\eta_s]. \tag{11}$$

In terms of these new variables the BECF reads as

$$C(\Delta k; K) \simeq 1 + \frac{|\,\tilde{S}(\Delta k, K)\,|^2}{|\,\tilde{S}(0, K)\,|^2} \simeq 1 + \lambda_*(K) \frac{|\,\tilde{S}_{c,*}(Q_\tau, Q_\eta, Q_{out}, Q_{side})\,|^2}{|\,\tilde{S}_{c,*}(0,0,0,0)\,|^2}. \tag{12}$$

At this level, the shape of the BECF can be rather complicated, it may have non-Gaussian, non-factorizable structure. Gaussian approximation to eq. (12) may break down as discussed in more detail in the Appendix of ref.[9].

5. Mixing Angle for HBT

The BECF-s are frequently[28] but not exclusively[29] parameterized by some version of the Gaussian approximation. The out-longitudinal cross-term of BECF has also been

discovered in this context recently[16]. In order to identify how this term may come about, let us assume that

$$S_{c,*}(\tau, \eta, r_x, r_y) = H_*(\tau)\, G_*(\eta)\, I_*(r_x, r_y). \tag{13}$$

In Gaussian approximation one also assumes that

$$H_*(\tau) \propto \exp(-(\tau - \tau_s)^2/(2\Delta\tau_*^2)), \tag{14}$$
$$G_*(\eta) \propto \exp(-(\eta - \eta_s)^2/(2\Delta\eta_*^2)), \tag{15}$$
$$I_*(r_x, r_y) \propto \exp(-((r_x - r_{x,s})^2 + (r_y - r_{y,s})^2)/(2R_*^2)). \tag{16}$$

The corresponding BECF is given by a diagonal form as

$$C(\Delta k; K) = 1 + \lambda_* \exp(-Q_\tau^2 \Delta\tau_*^2 - Q_\eta^2 \tau_s^2 \Delta\eta_*^2 - Q_t^2 R_*^2). \tag{17}$$

This diagonal form shall be transformed to an off-diagonal one if one introduces the kinematic relations between the variables Q_τ, Q_η and the variables Q_{out}, Q_L. In the HBT coordinate system[27] one finds

$$C(\Delta k; K) = 1 + \lambda_* \exp(-R_{side}^2 Q_{side}^2 - R_{out}^2 Q_{out}^2 - R_L^2 Q_L^2 - 2R_{out,L}^2 Q_{out} Q_L) \tag{18}$$
$$R_{side}^2 = R_*^2, \tag{19}$$
$$R_{out}^2 = R_*^2 + \delta R_{out}^2, \tag{20}$$
$$\delta R_{out}^2 = \beta_t^2(\cosh^2[\eta_s]\Delta\tau_*^2 + \sinh^2[\eta_s]\tau_s^2\Delta\eta_*^2), \tag{21}$$
$$R_L^2 = (\beta_L \sinh[\eta_s] - \cosh[\eta_s])^2 \tau_s^2 \Delta\eta_*^2 + (\beta_L \cosh[\eta_s] - \sinh[\eta_s])^2 \Delta\tau_*^2, \tag{22}$$
$$R_{out,L}^2 = (\beta_t \cosh[\eta_s](\beta_L \cosh[\eta_s] - \sinh[\eta_s]))\Delta\tau_*^2 +$$
$$(\beta_t \sinh[\eta_s](\beta_L \sinh[\eta_s] - \cosh[\eta_s]))\tau_s^2 \Delta\eta_*^2. \tag{23}$$

Note that the effective temporal duration, $\Delta\tau_*$ and the effective longitudinal size, $\tau_s \Delta\eta_*$ appear in a mixed form in the BECF parameters δR_{out}^2, R_L^2 and $R_{out,L}^2$, and their mixing is controlled by the value of the parameter η_s. These results simplify a lot[9] in the LCMS, the Longitudinally Co-Moving System[30], where $\beta_L = 0$:

$$\delta R_{out}^2 = \beta_t^2(\cosh^2[\eta_s]\Delta\tau_*^2 + \sinh^2[\eta_s]\tau_s^2\Delta\eta_*^2), \tag{24}$$
$$R_L^2 = \cosh^2[\eta_s]\tau_s^2\Delta\eta_*^2 + \sinh^2[\eta_s]\Delta\tau_*^2, \tag{25}$$
$$R_{out,L}^2 = -\beta_t \sinh[\eta_s]\cosh[\eta_s](\Delta\tau_*^2 + \tau_s^2\Delta\eta_*^2). \tag{26}$$

Let us define the Longitudinal Saddle-Point System (LSPS) to be the frame where $\eta_s(m_t) = 0$. In LSPS one finds that

$$\delta R_{out}^2 = \beta_t^2 \Delta\tau_*^2, \tag{27}$$
$$R_L^2 = \tau_s^2 \Delta\eta_*^2 + \beta_L^2 \Delta\tau_*^2, \tag{28}$$
$$R_{out,L}^2 = \beta_t \beta_L \Delta\tau_*^2. \tag{29}$$

Introducing $Q_0 = \beta_t Q_{out} + \beta_L Q_L$ and $Q_t = \sqrt{Q_{out}^2 + Q_{side}^2}$ the BECF can be rewritten in LSPS as

$$C(\Delta k; K) = 1 + \lambda_* \exp(-\Delta\tau_*^2 Q_0^2 - \tau_s^2 \Delta\eta_*^2 Q_L^2 - R_*^2 Q_t^2). \tag{30}$$

Thus the out-long cross-term can be diagonalized in the LSPS frame[18, 9]. The cross term should be small in LCMS if $\eta_s^{LCMS} << 1$ i.e. if $\mid y - y_0 \mid << \Delta y$ [9]. Since the size of the cross-term is controlled by the value of η_s in any given frame, it follows that η_s is the *cross-term generating hyperbolic mixing angle*[9] for cylindrically symmetric, longitudinally expanding finite systems which satisfy the factorization of eq. (13). The physical meaning of this hyperbolic mixing angle η_s is illustrated on Figure 1.

6. A New Class of Analytically Solvable Models

For high energy heavy ion reactions, we model the emission function of the core with an emission function described in detail in ref.[9]. This corresponds to a Boltzmann approximation to the local momentum distribution of a longitudinally expanding finite system which expands into the transverse directions with a transverse flow, which is non-relativistic at the maximum of particle emission. The decrease of the temperature distribution $T(x)$ in the transverse direction is controlled by parameter a, the strength of the transverse flow is controlled by parameter b. Parameter d controls the strength of the change of the local temperature during the course of particle emission[9]. If all these parameters vanish, $a = b = d = 0$, one recovers the case of longitudinally expanding finite systems with $T(x) = T_0$ with no transverse flow, as discussed in ref.[6], if $a = d = 0 \neq b$ the model of ref.[16] is obtained.

Specifically, we study the following model emission function for high energy heavy ion reactions:

$$S(x;K)\,d^4x = \frac{g}{(2\pi)^3} m_t \cosh(\eta - y)\, H(\tau) \times \exp\left(-\frac{K\cdot u(x)}{T(x)} + \frac{\mu(x)}{T(x)}\right) d\tau\, \tau_0 d\eta\, dr_x dr_y. \quad (31)$$

Here g is the degeneracy factor, the pre-factor $m_t \cosh(\eta - y)$ corresponds to the flux of the particles through a $\tau = const$ hyper-surface according to the Cooper-Frye formula [31] and the four-velocity $u(x)$ is

$$u(x) = \left(\cosh(\eta)\left(1 + b^2\frac{r_x^2+r_y^2}{\tau_0^2}\right)^{(1/2)}, b\frac{r_x}{\tau_0}, b\frac{r_y}{\tau_0}, \sinh(\eta)\left(1 + b^2\frac{r_x^2+r_y^2}{\tau_0^2}\right)^{(1/2)}\right)$$
$$\simeq \left(\cosh(\eta)\left(1 + b^2\frac{r_x^2+r_y^2}{2\tau_0^2}\right), b\frac{r_x}{\tau_0}, b\frac{r_y}{\tau_0}, \sinh(\eta)\left(1 + b^2\frac{r_x^2+r_y^2}{2\tau_0^2}\right)\right), \quad (32)$$

which describes a scaling longitudinal flow field merged with a linear transverse flow profile. The transverse flow is assumed to be non-relativistic in the region where there is significant contribution to particle production. The local temperature distribution $T(x)$ at the last interaction points is assumed to have the form

$$\frac{1}{T(x)} = \frac{1}{T_0}\left(1 + a^2\frac{r_x^2+r_y^2}{2\tau_0^2}\right)\left(1 + d^2\frac{(\tau-\tau_0)^2}{2\tau_0^2}\right), \quad (33)$$

and the local rest density distribution is controlled by the chemical potential $\mu(x)$ for which we have the ansatz

$$\frac{\mu(x)}{T(x)} = \frac{\mu_0}{T_0} - \frac{r_x^2+r_y^2}{2R_G^2} - \frac{(\eta-y_0)^2}{2\Delta\eta^2}. \quad (34)$$

The parameters R_G and $\Delta\eta$ control the density distribution with finite geometrical sizes. The proper-time distribution of the last interaction points is assumed to have the following simple form:

$$H(\tau) = \frac{1}{(2\pi\Delta\tau^2)^{(1/2)}} \exp\left(-(\tau-\tau_0)^2/(2\Delta\tau^2)\right). \quad (35)$$

The parameter $\Delta\tau$ stands for the width of the freeze-out hyper-surface distribution, i.e. the emission is from a layer of hyper-surfaces which tends to an infinitely narrow hyper-surface in the $\Delta\tau \to 0$ limit.

The integrals of the emission function are evaluated using the saddle-point method [22, 11, 17]. The saddle-point coincides with the maximum of the emission function, parameterized by $(\tau_s, \eta_s, r_{x,s}, r_{y,s})$. These coordinate values solve simultaneously the equations

$$\frac{\partial S}{\partial\tau} = \frac{\partial S}{\partial\eta} = \frac{\partial S}{\partial r_x} = \frac{\partial S}{\partial r_y} = 0. \quad (36)$$

These saddle-point equations are solved in the LCMS, the longitudinally Co-moving system, for $\eta_s^{LCMS} << 1$ and $r_{x,s} << \tau_0$. The approximations are self-consistent if $\mid Y - y_0 \mid << 1 + \Delta\eta^2 m_t/T_0 - \Delta\eta^2$ and $\beta_t << \tau_s^2\Delta\eta_T^2/(bR_*^2)$ which can be simplified for the considered model as $\beta_t = p_t/m_t << (a^2+b^2)/b/\max(1,a,b)$. The transverse flow is non-relativistic at the saddle-point if $\beta_t << (a^2+b^2)/b^2/\max(1,a,b)$. We assume that $\Delta\tau < \tau_0$ so that the Fourier-integrals involving $H(\tau)$ in the $0 \leq \tau < \infty$ domain can be extended to the $-\infty < \tau < \infty$ domain. The radius parameters are evaluated here to the leading order in $r_{x,s}/\tau_0$. Thus terms of $\mathcal{O}(r_{x,s}/\tau_0)$ are neglected, however we keep all the higher-order correction terms arising from the non-vanishing value of η_s in the LCMS.

For the model of eq. (31) the saddle point approximation for the integrals leads to an effective emission function which can be factorized similarly to eq. (13). Thus the radius parameters of the model are expressible in terms of the homogeneity lengths $\Delta\eta_*, R_*, \Delta\tau_*$ and the position of the saddle point η_s i.e. the cross-term generating hyperbolic mixing angle. The saddle-point in LCMS is given by $\tau_s = \tau_0$, $\eta_s^{LCMS} = (y_0 - Y)/(1 + \Delta\eta^2(1/\Delta\eta_T^2 - 1))$, $r_{x,s} = \beta_t b R_*^2/(\tau_0\Delta\eta_T^2)$ and $r_{y,s} = 0$.

7. Geometrical vs. Thermal Length Scales for BECF-s

The parameters of the correlation function are related by eqs. (18-29) to the parameters R_*, $\Delta\tau_*$ and $\tau_s\Delta\eta_*$ which in turn are given by

$$\frac{1}{R_*^2} = \frac{1}{R_G^2} + \frac{1}{R_T^2}\cosh[\eta_s], \quad (37)$$

$$\frac{1}{\Delta\eta_*^2} = \frac{1}{\Delta\eta^2} + \frac{1}{\Delta\eta_T^2}\cosh[\eta_s] - \frac{1}{\cosh^2[\eta_s]}, \quad (38)$$

$$\frac{1}{\Delta\tau_*^2} = \frac{1}{\Delta\tau^2} + \frac{1}{\Delta\tau_T^2}\cosh[\eta_s]. \quad (39)$$

Here the geometrical sizes are given by R_G, the transverse size, $\Delta\eta$, the width of space-time rapidity distribution and $\Delta\tau$, the duration around the mean emission time $\tau_s = \tau_0$. The hyperbolic mixing angle $\eta_s \approx 0$ at mid-rapidity y_0 [9], where also the out-long cross-term[16] vanishes. The thermal length-scales (subscript $_T$) are given by

$$R_T^2 = \frac{\tau_0^2}{a^2+b^2}\frac{T_0}{M_t}, \qquad \Delta\eta_T^2 = \frac{T_0}{M_t}, \qquad \Delta\tau_T^2 = \frac{\tau_0^2}{d^2}\frac{T_0}{M_t}. \quad (40)$$

The transverse mass of the pair is denoted by $M_t = \sqrt{K_0^2 - K_L^2}$.

These analytic expressions indicate that the BECF views only a part of the space-time volume of the expanding systems, which implies that even a complete measurement of the parameters of the BECF as a function of the mean momentum K may not be sufficient to determine uniquely the underlying phase-space distribution.

It is timely to emphasize at this point that the parameters of the Bose-Einstein correlation function coincide with the (rapidity and transverse mass dependent) *lengths of homogeneity*[22] in the source, which can be identified with that region in coordinate space where particles with a given momentum are emitted from. The lengths of homogeneity for thermal models can be obtained from basically two type of scales referred to as 'thermal' and 'geometrical' scales.

The thermal scales originate from the factor $\exp(-p\cdot u(x)/T(x))$, where $u(x)$ is the four-velocity field. This is to be contrasted to the 'geometrical' scales, which originate from the $\exp(\mu(x)/T(x))$ factor which controls the density distribution[9]. Here $\mu(x)$ stands for the chemical potential. How do the changes of the temperature in the transverse or temporal directions induce transverse mass dependent thermal radius or thermal duration parameters? See ref. [10] for illustration.

As a consequence of possible temporal changes of the local temperature, we find that the effective duration of the particle emission $\Delta\tau_*$ may become transverse mass dependent and for sufficiently large values of the transverse mass this parameter may become vanishingly small. The reason for this new effect is rather simple: Particles with a higher transverse mass are effectively emitted in a time interval when the local temperature (boosted by the transverse flow) is higher than the considered value for m_t. If the local temperature changes during the course of particle emission, the effective emission time for high transverse mass particles shall be smaller than the effective emission time of particles with lower transverse mass values.

For a more detailed analysis of the model the reader is referred to ref.[9, 32], where it is pointed out that under certain conditions the parameters of the Bose-Einstein correlation function may obey an M_t-scaling: $R_{side} \simeq R_{out} \simeq R_L \propto 1/\sqrt{M_t}$.

8. Results for the Invariant Momentum Distributions

The IMD plays a *complementary role* to the measured Bose-Einstein correlation function [6, 5, 8]. Thus a *simultaneous analysis* of the Bose-Einstein correlation functions and the IMD may reveal information both on the temperature and flow profiles and on the geometrical sizes.

For the considered model, eq. (31), the invariant momentum distribution can be calculated in such a manner, that the Cooper-Frye pre-factor $m_t\cosh(\eta - y)$ is kept exactly and the saddle-point approximation is applied to the remaining Boltzmann and proper-time factors, $\exp(-p\cdot u/T(x) + \mu(x)/T(x))H(\tau)$. This calculation yields:

$$N_{1,c}(\mathbf{p}) = \frac{g}{(2\pi)^3}(2\pi\overline{\Delta\eta_*}^2\tau_0^2)^{1/2}(2\pi\overline{R_*}^2)\frac{\overline{\Delta\tau_*}}{\Delta\tau}\, m_t\cosh(\overline{\eta_s})\,\exp(+\overline{\Delta\eta_*}^2/2)\times \exp(-p\cdot u(\overline{x}_s)/T(\overline{x}_s) + \mu(\overline{x}_s)/T(\overline{x}_s)). \quad (41)$$

The quantities $\overline{\Delta\eta_*}^2$ and $\overline{\eta_s}$ are defined as

$$\frac{1}{\overline{\Delta\eta_*}^2} = \frac{1}{\Delta\eta^2} + \frac{1}{\Delta\eta_T^2}\cosh[\overline{\eta_s}], \qquad \overline{\eta_s} = \frac{(y_0 - y)}{1 + \Delta\eta^2/\Delta\eta_T^2} \quad (42)$$

and the modified saddle-point is located in LCMS at $\overline{\tau}_s = \tau_s = \tau_0$, $\overline{\eta_s}$, $\overline{r_{x,s}} = \beta_t b\overline{R_*}^2/(\tau_0\Delta\eta_T^2)$ and $\overline{r_{y,s}} = 0$. The modified radius and life-time parameters can be obtained by evaluating the R_* and $\Delta\tau_*$ parameters at the space-time rapidity coordinate of the modified saddle-point, $\overline{R_*} = R_*(\eta_s^{LCMS} \to \overline{\eta_s})$ and $\overline{\Delta\tau_*} = \Delta\tau_*(\eta_s^{LCMS} \to \overline{\eta_s})$. Thus the modified quantities (indicated by over-line) differ from the unmodified parameters of the saddle-point approximation by the contributions of the Cooper-Frye pre-factor. Note, that $\overline{R_*} \simeq R_*$ and $\overline{\Delta\tau_*} \simeq \Delta\tau_*$ in the mid-rapidity region, where $\eta_s^{LCMS}, \overline{\eta_s} << 1$.

In eq. (41) the exact shape of the four-velocity field can be used, which is given in the first line of eq. (32). When evaluating $\mu(\overline{x_s})/T(\overline{x_s})$ in any frame, the invariant difference $\overline{\eta_s} - y_0^{LCMS} = \overline{\eta_s} + y - y_0$ should be used.

The momentum distribution as given in eq. (41) can be rewritten into a more explicit shape, which is more suitable for analytic study. This can be done if one neglects terms of $\mathcal{O}(\overline{r_{x,s}}^3/\tau_0^3)$ in the exponent, which is the same order of accuracy which has been utilized for the solution of the saddle-point equations. Further, a term in the exponent $(m_t/T_0)\cosh(\overline{\eta_s})$ is approximated by its second-order Taylor expansion, $(m_t/T_0)(1 + 0.5\overline{\eta_s}^2)$. These approximations yield

$$N_{1,c}(\mathbf{p}) = \frac{g}{(2\pi)^3}(2\pi\overline{\Delta\eta_*}^2\tau_0^2)^{1/2}(2\pi R_*^2)\frac{\Delta\tau_*}{\Delta\tau}\, m_t\cosh(\overline{\eta_s})\,\exp(+\overline{\Delta\eta_*}^2/2)\times \exp(\mu_0/T_0)\,\exp\left(-\frac{(y-y_0)^2}{2(\Delta\eta^2+\Delta\eta_T^2)}\right)\times \exp\left(-\frac{m_t}{T_0}\left(1 - f\frac{\beta_t^2}{2}\right)\right)\exp\left(-f\frac{m_t\beta_t^2}{2(T_0+T_G)}\right), \quad (43)$$

where the geometrical contribution to the effective temperature is given by $T_G(m_t) = T_0\, R_G^2/R_T^2(m_t) = (a^2+b^2)\, m_t\, R_G^2/\tau_0^2$ and the fraction f is defined as $f = b^2/(a^2+b^2)$, satisfying $0 \le f \le 1$. The following relations hold:

$$\Delta y^2(m_t) \;=\; \Delta\eta^2 + \Delta\eta_T^2(m_t) \qquad \text{and} \qquad \frac{1}{T_*} = \frac{f}{T_0 + T_G(m_t = m)} + \frac{1-f}{T_0}. \quad (44)$$

Thus e.g. the width $\Delta y^2(m_t)$ is dominated by the longer of the geometrical and thermal length scale, in contrast to the HBT radius parameters which are dominated by the shorter of these scales. That is why the IMD measurements can be considered to be complementary to the BECF data.

9. Analysis of Limitations

The simple analytic formulas presented in the previous sections are obtained in a saddle-point approximation for the evaluation of the space-time integrals. This approximation is known to converge to the exact result in the limit the integrated function develops a sufficiently narrow peak, i. e. both

$$\Delta\eta_*^2(y, m_t) << 1 \quad \text{and} \quad \Delta\tau_*^2(y, m_t)/\tau_s^2 << 1 \qquad (45)$$

are required. These in turn give a lower limit in m_t for the applicability of the formulas for the class of models presented in the previous section. These limits were studied analytically in ref. [9], here we analyze them numerically in the subsequent parts.

Compared to the condition (45), the condition of validity of the calculation of the invariant momentum distribution is less stringent, since one needs to satisfy only $\overline{\Delta\eta_*^2} << 1$. In the mid-rapidity region where NA44 data were taken, one has $\eta_s \simeq 0$ and for *finite* systems one finds $m_t >> T_0(2 - 1/\Delta\eta^2)$. Note that this estimated lower limit in m_t is extremely sensitive to the precise value of $\Delta\eta$ in the region $\Delta\eta \simeq 1/\sqrt{2} \approx 0.7$. For finite systems, the region of applicability of our results extends to lower values of m_t than for infinite systems which were recently studied in great detail in ref. [19]. An upper transverse momentum limit is obtained for the validity of the calculations from the requirement

$$r_{x,s}/\tau_0 \;<\; 1 \qquad (46)$$

or $r_{x,s}^2/\tau_0^2 << 1$. This condition and the requirement $b r_{x,s}/\tau_0 < 1$ has to be fulfilled simultaneously. Finally we note that the linearization of the saddle-point equations assumes that

$$\eta_s^{LCMS} < 1 \qquad (47)$$

and for the IMD calculations a less stringent condition $\overline{\eta_s} < 1$ was assumed.

When comparing to data, detailed numerical studies may be necessary [19] to check the precision of the saddle-point integration. In the subsequent chapters, we present these tests for the analytic results given above and indicate the numerically found validity or violation of the conditions given in this Chapter.

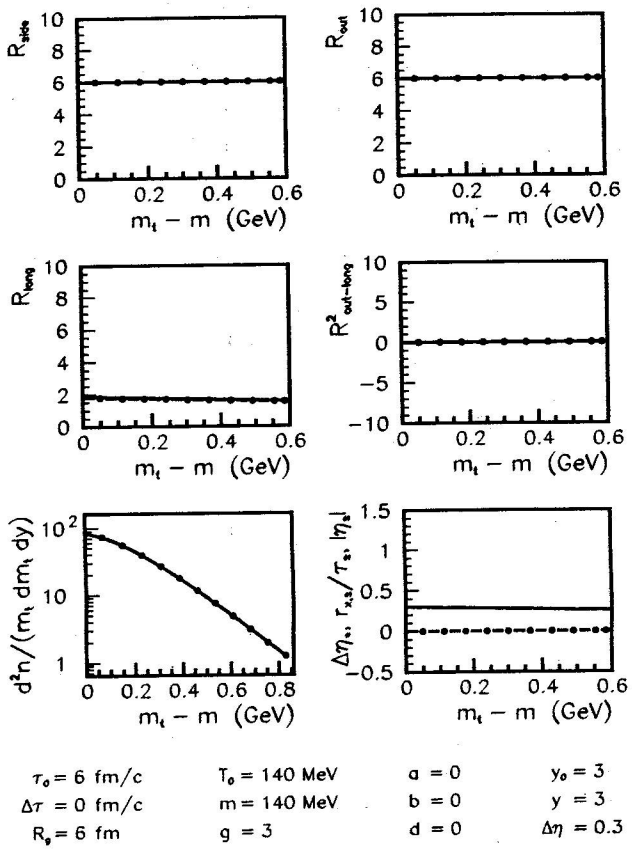

Fig. 2. BECF parameters in LCMS, the IMD and the essential 'small' parameters. Solid line shows the results of numerical integration, dash-dotted line indicates the analytical results. Note that the transverse flow is switched off and $T(x) = T_0$ as follows from $a = b = d = 0$. The longitudinal size is chosen to be small, $\Delta\eta = 0.3$. On the last sub-plot, solid line indicates $\Delta\eta_*$, dash-dotted line stands for $r_{x,s}/\tau_s$ and dashed line for η_s^{LCMS}. These quantities are required to satisfy $\Delta\eta_*^2 << 1$, $r_{x,s}^2/\tau_s^2 << 1$ and $\eta_s^{LCMS} << 1$. The other conditions, $\Delta\tau_*^2/\tau_s^2 << 1$ and $\overline{\Delta\eta_*^2} << 1$ are weaker conditions and thus not indicated on this and the subsequent plots.

10. Numerical test for the a = b = d = 0 case

Let us start the numerical analysis with a set of parameters, that satisfy both conditions (45) and (46). This is the reason for choosing $a = b = d = 0$ and $\Delta\eta = 0.3$ which guarantees that $\Delta\eta_* << 1$ is satisfied. We start the analysis at mid-rapidity, and devote the last chapter to studies in the target and projectile fragmentation region. Note that

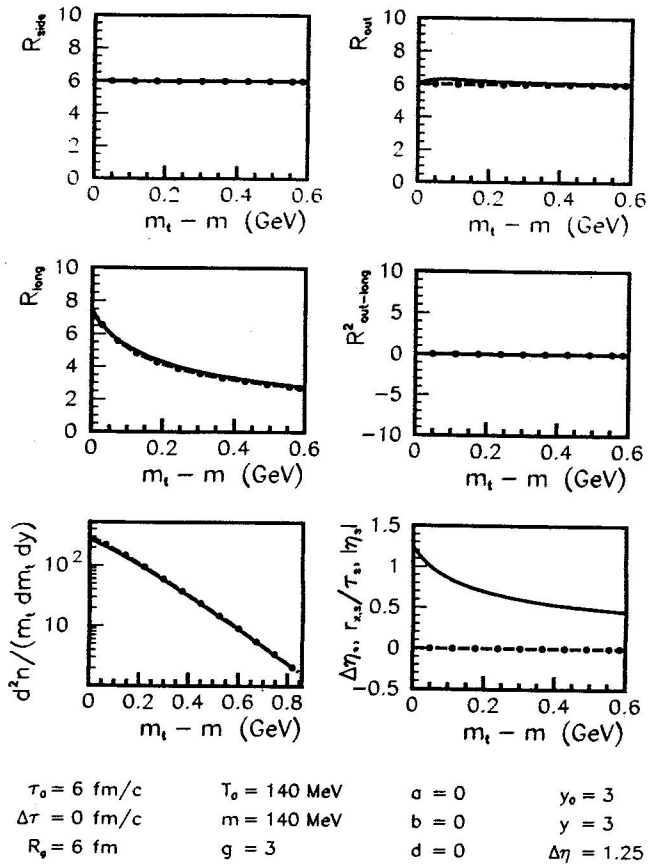

Fig. 3. Same as Figure 2, but with increased longitudinal size, $\Delta\eta = 1.25$. In the low-m_t region $\Delta\eta_*^2 \geq 1$, which results in a slight increase of the numerically calculated R_{out} component as compared to the analytical result.

the out-longitudinal cross-term [16] vanishes at mid-rapidity.

Due to the large number of model-parameters a rather comprehensive analysis is necessary and it is important to check the effects from various type of parameters.

As one can see on Figure 2 the agreement between the analytical results and the numerically evaluated radius parameters and IMD is almost perfect. Note that for the analytical calculations of the HBT radii in LCMS eqs. (18-29,37-39) were used, the IMD has been analytically evaluated both from the slightly more precise eq. (43) and from the more approximate eq. (41), both yielding results indistinguishable from the numerically integrated curve. For the numerical results on the HBT radii, we have evaluated the model-independent Gaussian radii in LCMS, as given in refs. [17, 16], for

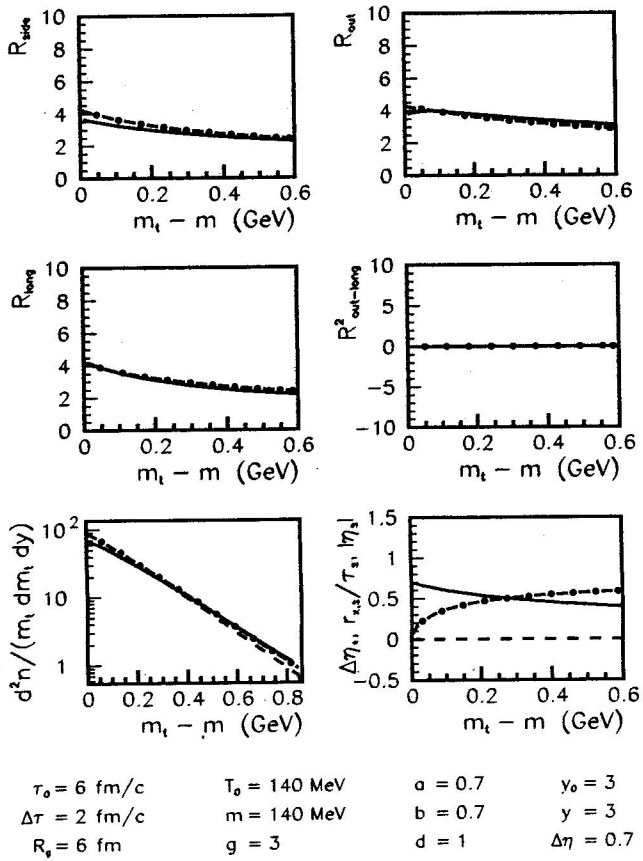

Fig. 4. Transverse flow, transverse and temporal temperature gradients are switched on. Parameters correspond to a scaling limiting case at mid-rapidity. The numerical integration (solid line) is performed for the approximate transverse flow profile. Dash-dotted line indicates the analytical results. For the IMD sub-plot, dashed line stands for the simplified analytical result, eq. (43), and dash-dotted line indicates the slightly more precise eq. (41).

the model emission function of eq. (31). For the numerical evaluation of the IMD, we have utilized eq. (2).

How significant is the limitation given by eq. (45)? Can we apply the analytical results to systems created at 200 AGeV bombarding energy, where $\Delta\eta \simeq 1.5$? According to Figures 3 and 6 the analytical results provide a good approximation even in this case, (note that Figure 6 is evaluated for $\Delta\eta = 1.5$ for $a, b, d \neq 0$). The relative error on these figures is maximal around $m_t = 240$ MeV for pions, being about 10 % for $\Delta\eta = 1.2$, 20 % for $\Delta\eta = 1.5$. These errors are characteristic for the R_{out} and R_{long} radius parameters.

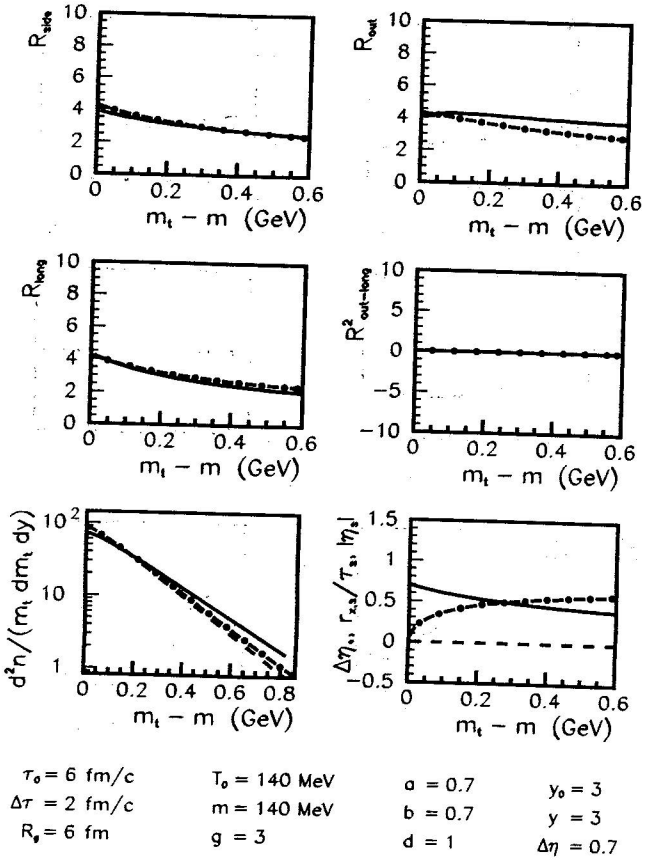

Fig. 5. Same as Figure 4, but now the numerical integration was performed with the exact transverse flow profile.

The side radius component and the spectrum is obtained with much smaller errors. The relative error of the analytical results vanishes with increasing m_t for this case. Thus the analytic approximations are reasonably good, sometimes excellent if $a = b = d = 0$ and $\Delta\eta \leq 1.5$.

11. Flow and Temperature Profile Effects

The cases with non-vanishing parameters a, b and d are studied in this chapter. Figures 4 and 5 compare the analytical results with the numerical ones for $\Delta\eta = 0.7$ case, Figure 6 shows the same for $\Delta\eta = 1.5$. The model parameters of these figures correspond to an approximate m_t scaling for the radius parameters of the BECF. On Figure 5, the model

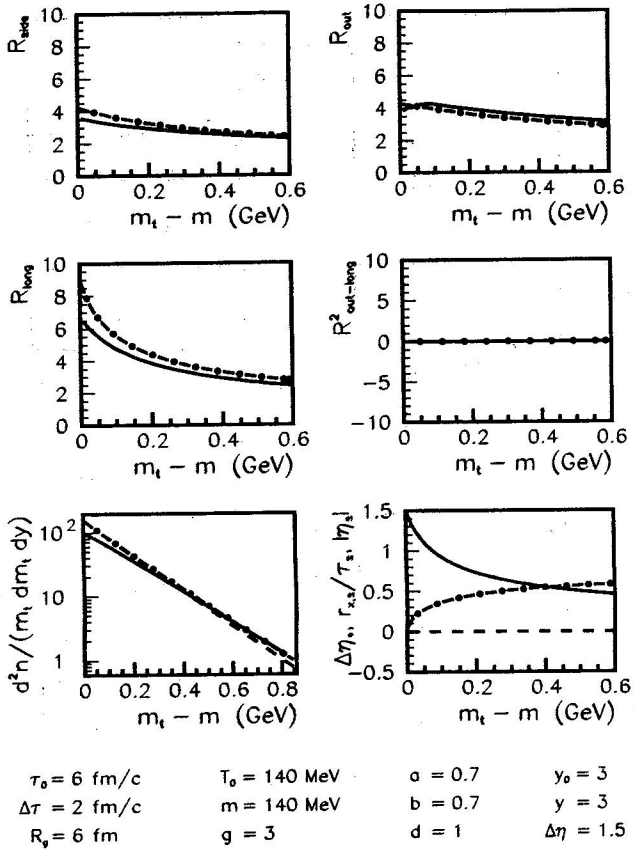

Fig. 6. Same as Figure 4, but the longitudinal size of the system is increased.

was integrated numerically utilizing the exact flow profile, as given by the first line of eq. (32). On Figures 4 and 6, the approximation given in the second line of eq. (32) has been performed before the numerical integration. In this case, the high m_t limit of the analytical calculations corresponds to that of the numerical one, as it should because the radius parameters of saddle-point integration decrease with increasing m_t and thus the precision of the saddle-point integration increases with increasing value of m_t.

In the region of $m_t - m \leq 200$ MeV, the relative error of the analytical calculations for the HBT radius parameters is about 10 %. In case of the IMD the relative error refers to that of the slope parameter, which is approximately 10 % on Figures 4 and 6.

It is worth comparing Figure 4 with Figure 5. The analytical curves on these figures are the same, but the flow profile eq. (32) is exact on Figure 5, while the approximation

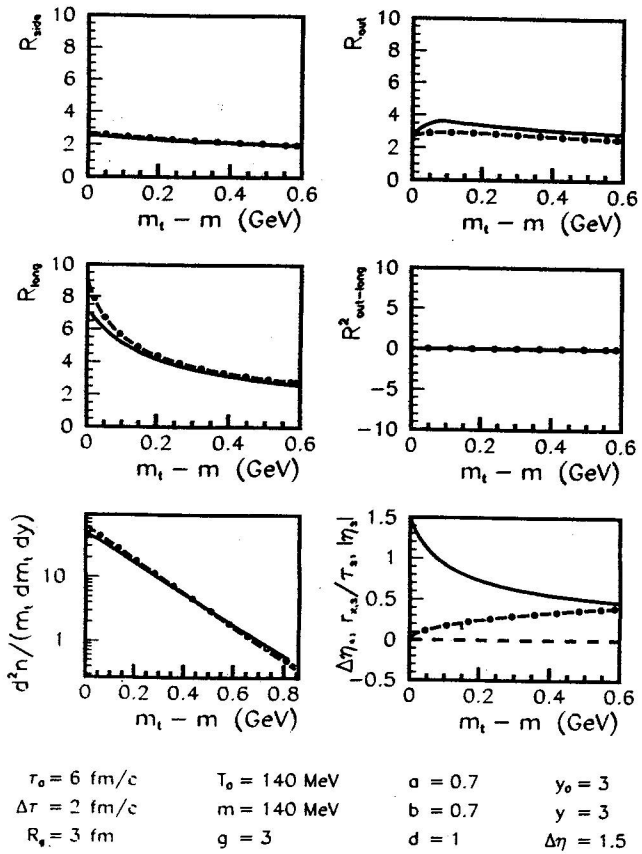

Fig. 7. Numerical integration done with exact flow profile, case $R_G < R_T(m)$ for pions.

in eq. (32) was performed before the numerical integration on Figure 4. The side and the longitudinal radius parameters are not changed significantly, however the high m_t part of the spectrum and the out radius parameter is enhanced, increasing the deviation between numerical and analytical results to about 20 - 25 % in the kinematic region $m_t - m < 600$ MeV. Note that the two analytic approximations for the spectrum, eqs. (41) and (43) yield slightly different results, as indicated by the dashed and dash-dotted lines on the IMD part of the Figures, respectively.

12. Pions vs. Kaons

One expects that the precision of the calculation is increased for particles heavier than pions, because the thermal scales and thus the radius parameters decrease with increasing transverse mass. This is indeed the case, as indicated by Figures 7 - 10. When evaluating the numerical integrals for these figures, as well as Figures 11 - 16, the exact flow profile has been utilized.

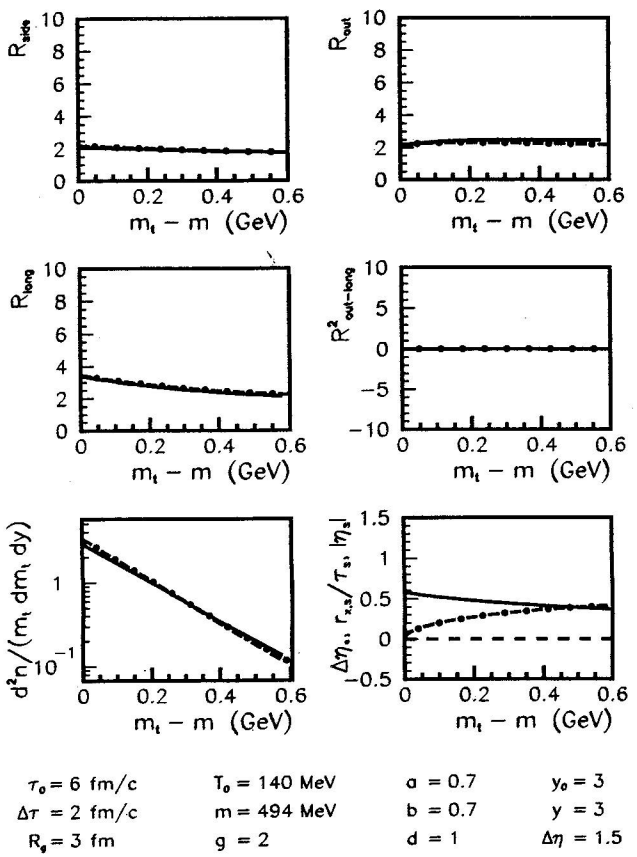

Fig. 8. Same parameters as for Figure 7, but for kaons.

The radius parameters are dominated by the geometrical ones on Figures 7 and 8, resulting in a weaker m_t dependence, while on Figures 9 and 10 the HBT radius parameters are dominated by the thermal scales since $R_G > R_T(m)$ for pions, and the radius parameters satisfy approximate m_t scaling. On these figures, the precision of the analytic results is nowhere worse than 20 %, in some cases especially for kaons and for the side and the longitudinal radius parameter at higher m_t the relative errors become less than 5 %.

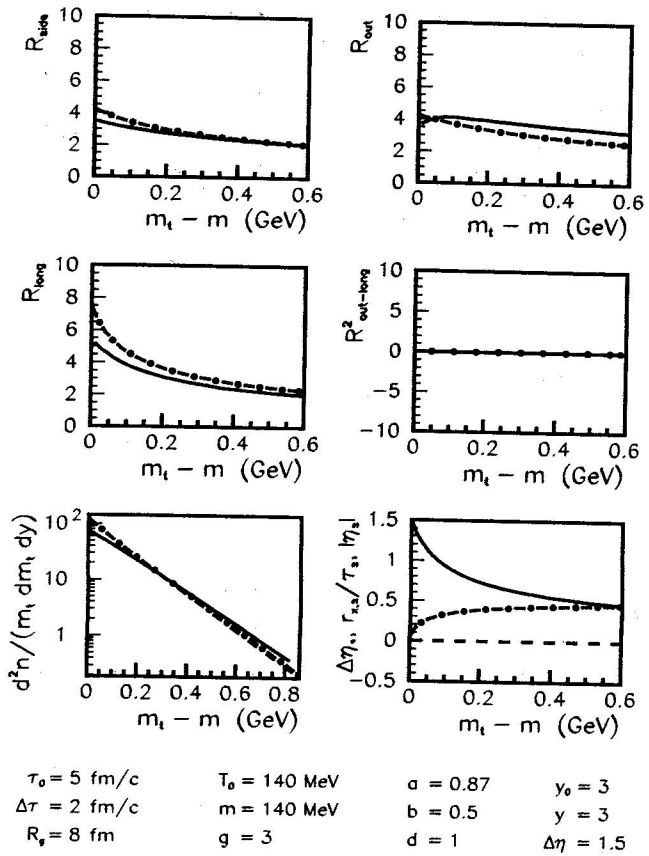

Fig. 9. Numerical integration done with exact flow profile, case $R_G > R_T(m)$ for pions.

13. Beyond the Limitations

We have already seen that the conditions for the smallness of $\Delta\eta_*$ are automatically satisfied at higher m_t thus the requirement (45) is not very important. On the previous graphs, we have shown figures where the other condition for the validity of the calculation, eq. (46) has been satisfied. In this chapter we violate this condition eq. (46) by a seemingly innocent change in the values of the parameters a, b, R_G and τ_0. This way the saddle-point $x_s(m_t)$ deviates more and more from zero and it moves outside the region where the linearization of the saddle-point equations is allowed. Thus the analytical approximations break down as illustrated on Figures 11 - 13. The most serious defect is observable in the sub-plots indicating the IMD. The slope-parameter is very badly estimated by the analytical results if the condition (46) is violated. A good numerical

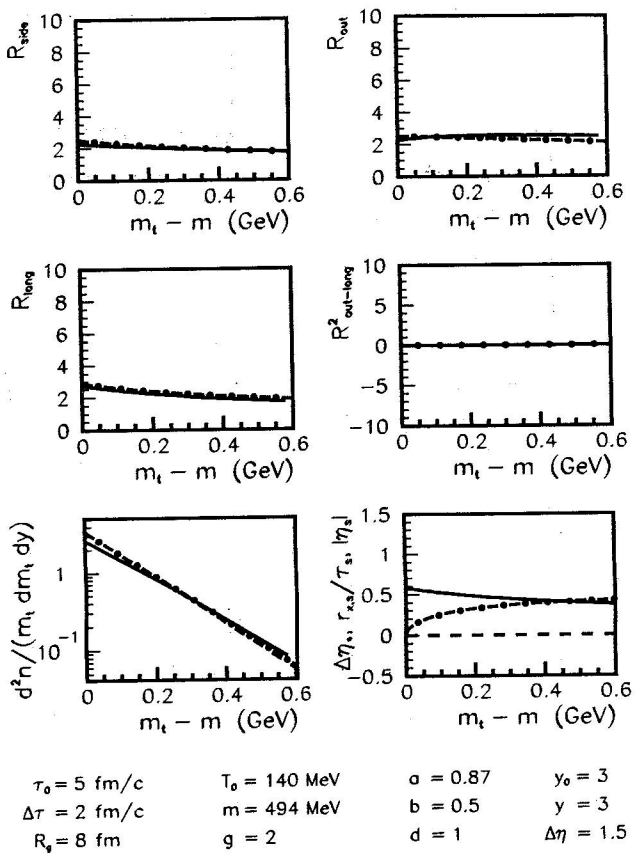

Fig. 10. Same parameters as for Figure 9, but for kaons.

interpretation of the condition (46) can thus be formulated as $r_{x,s}/\tau_0 \leq 0.6$. (Here we assume $b \leq 1$.) If $r_{x,s}/\tau_0 \leq 0.6$, the numerical and analytical results are in 10 -20 % agreement at mid-rapidity, however if $r^2_{x,s}/\tau^2_0 > 0.5$, the reliability of the analytic calculation is lost. The precision of model calculations for pions are very sensitive to whether this condition is well satisfied or violated.

Note that our analysis has been performed with $T_0 = 140$ MeV fixed. Lower values of T_0 improve the agreement between the analytical results and the numerical ones, while larger values of T_0 in general make the deviations larger in a given kinematic region.

Surprisingly, the HBT parameters for kaons are well reproduced even if $r^2_{x,s}/\tau^2_0 \approx 0.5$, except the R_{out} radius parameter at high m_t. For pions, the relative error on

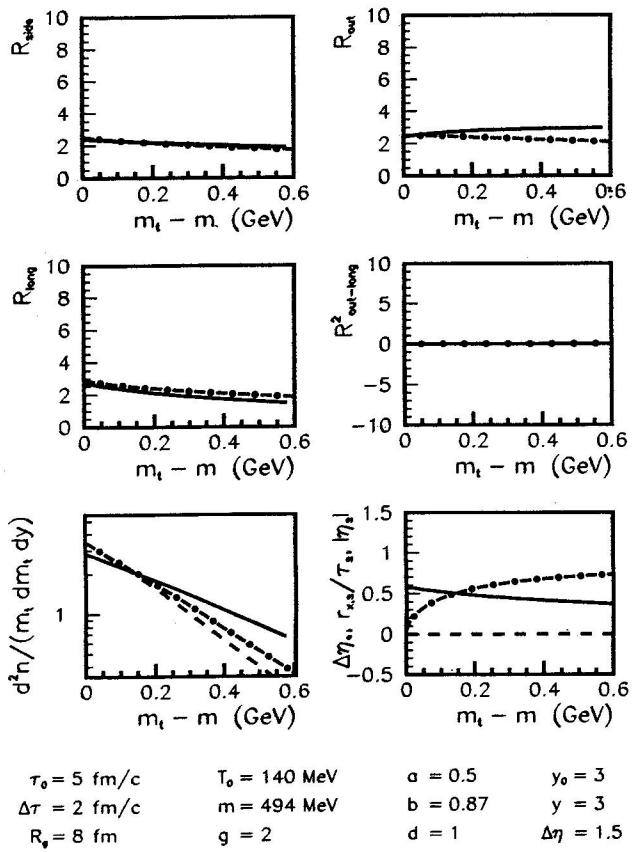

Fig. 11. Results for kaons, using a parameter set where the limitation $x_s(m_t)/\tau_0 << 1$ is violated: $x_s(m_t)/\tau_0 \geq 0.6$.

the radius parameters may reach 50 % for the side and the longitudinal momentum component, while it may reach 100% for the out radius component. Thus the condition of eq. (46) is substantial, it is mandatory to check it before concluding about the validity of the analytical approximations e.g. in a given data analysis.

14. Departure from Mid-Rapidity

Finally we turn our attention to LCMS radius parameters and IMD results off the mid-rapidity region. We use such parameters that the analytical approximations are precise to $10 - 20$ % relative errors at mid-rapidity. For $y \neq y_0$, the out-longitudinal cross-term picks up non-vanishing values. This cross-term must vanish at $m_t = m$, it develops a

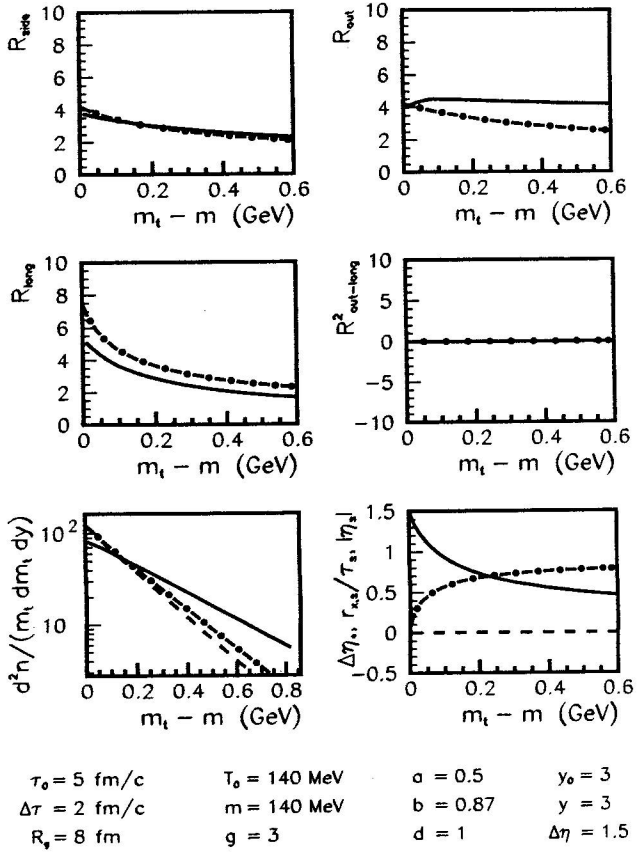

Fig. 12. Results for pions, using a parameter set where the limitation $x_s(m_t)/\tau_0 << 1$ is violated.

large modulus around $m_t - m = 50$ MeV, which decreases fast with increasing value of m_t, Figures 14 - 16. Surprisingly, the precision of the analytical approximations for side, longitudinal radius parameters and for the IMD is *improved* by moving one or two units away from the mid-rapidity. This is due to the fact that $r_{x,s}$, R_*, $\Delta\eta_*$ and $\Delta\tau_*$ all decrease with increasing η_s which corresponds to increasing values of $| y - y_0 |$. Figure 15 indicates that the analytic calculations may remain reliable even if $y = 1$ for a source centered around $y_0 = 3$ and having a width $\Delta\eta = 1.5$, except the analytical result for the cross term in the low m_t region. However, the analytical results for the cross-term are below the 20 % relative error limit if $m_t - m \geq 150$ MeV or if $\Delta\eta \leq 0.7$. With other words, the deviation of the analytical result for the cross-term from its numerically calculated value decreases very fast with increasing m_t. Figures 14 - 16 indicate, that

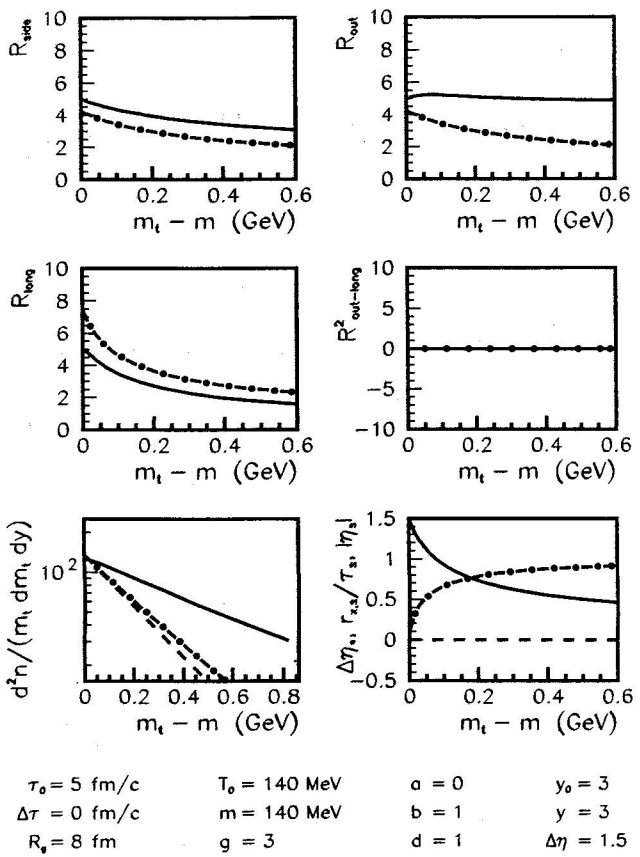

Fig. 13. Another violation of the limitation $x_s(m_t)/\tau_0 << 1$, using $a = 0$ and $b = 1$.

the analytical results for R_{side}, R_{long} and the IMD can provide an approximation with as small as 5 - 10 % relative error, for R_{out} with 15 % relative error even if the departure from mid-rapidity is substantial, $| y - y_0 | \simeq 2\Delta\eta$. According to Figure 16 the analytical approximations are reliable for $m_t - m > 150$ MeV if $y = 6$, for lower values of m_t the longitudinal saddle-point η_s^{LCMS} is badly determined, due to the break-down of the linearized saddle-point equations.

15. Summary and Conclusions

We have presented a detailed numerical testing of the analytical approximations, as were given in [9] describing a three-dimensionally expanding, cylindrically symmetric, finite system. We find that the typical precision of the analytical approximations is

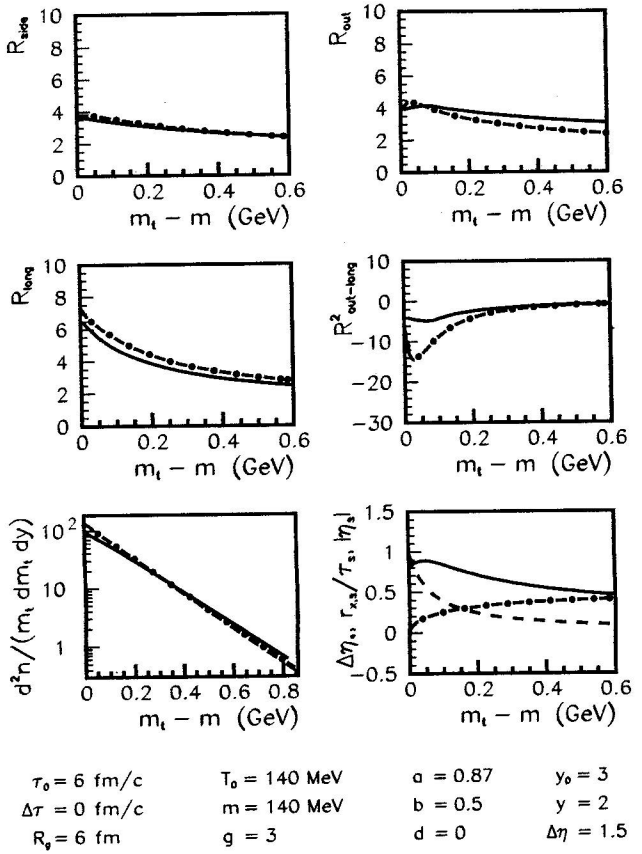

Fig. 14. Numerical versus analytical results at $y = 2$. Note that mid-rapidity is located at $y_0 = 3$ and that the longitudinal size is given by $\Delta\eta = 1.5$. Note that $\Delta\tau = 0$ fm/c.

characterized by a relative error of about 10 - 20 %, but in some cases much more precise agreement is found. Numerically, we have found that the analytic approximations are reliable (within 10 -20 % relative errors) if the transverse position of the saddle-point satisfies $r_{x,s}/\tau_0 \leq 0.6$ in some kinematic region. Numerically we find that this condition is the most sensitive among all the analytically found conditions for the validity of the analytical approximations, and a small violation of this condition may result in large deviations between the analytical and numerical values. This corresponds to the break-down of the linearized saddle-point equations in this case.

Surprisingly, we find that moderate deviation from mid-rapidity *improves* the agreement between the analytical results and the numerically found values for the HBT

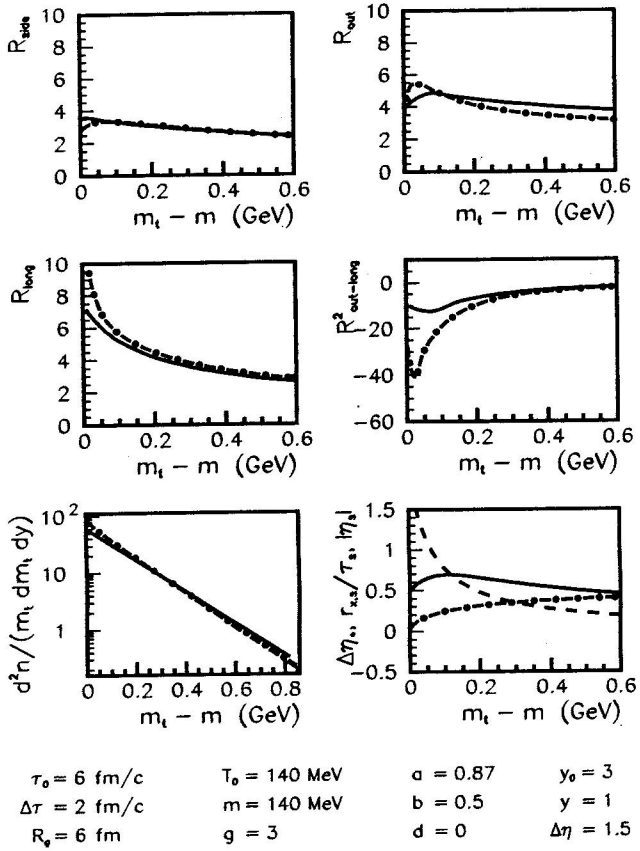

Fig. 15. Same as Figure 14, but in the target fragmentation region $y = 1$ and for $\Delta\tau = 2fm/c$.

radius parameters and the invariant momentum distribution. This is due to the decrease of the transverse position of the saddle-point and the decrease of the effective source sizes with increasing deviation from mid-rapidity $| y - y_0 |$. For large deviations from mid-rapidity, e.g. $| y - y_0 | = 2\Delta\eta$, the analytical values for the cross-term and for the HBT radius parameters are found to be unreliable in the $m_t - m \leq 150$ MeV interval. However, for larger values of $m_t - m$ the HBT radius parameters, including even the cross-term, are reproduced correctly even at $y = 6$. This lower limit $m_t > 150$ MeV corresponds to the requirement $\eta_s^{LCMS} \leq 0.9$.

In conclusion, we find that the analytical results are more reliable than expected before, since they are reliable in a fairly large rapidity interval. When comparing the analytic results to data, one has to check if the transverse position and the space-time

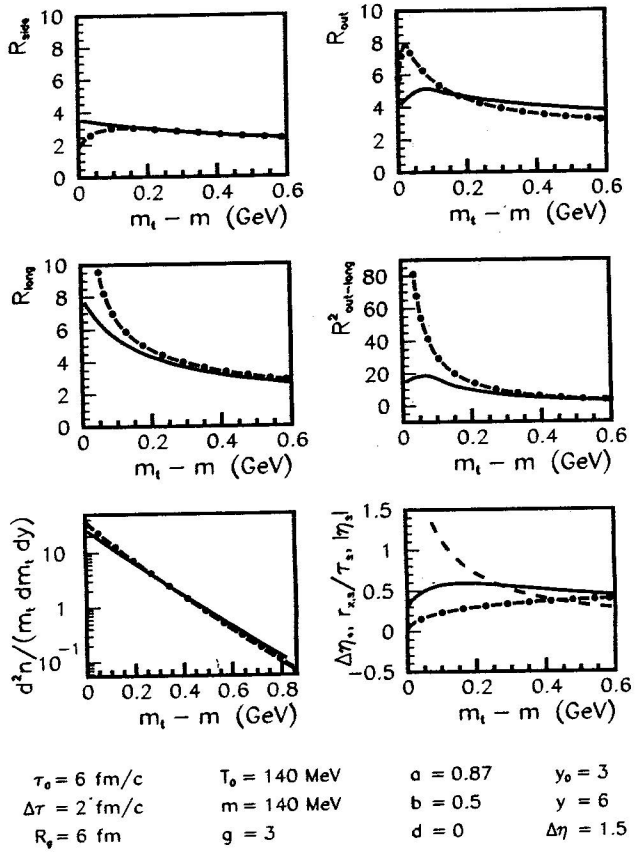

Fig. 16. Same as Figure 15, for $y = 6$.

rapidity of the saddle-point is not too large in LCMS. The essential numerical conditions of consistency are found to be $r_{x,s}/\tau_0 < 0.6$ and $\eta_s^{LCMS} \leq 0.9$.

Acknowledgments The authors would like to thank B. Tomášik for his contributions to the model-testing and for his careful reading of the manuscript. Cs. T. would like to thank Ján Pišút and the Organizing Committee for invitation and local support at the Bratislava School and Workshop on Heavy Ion Physics. He thanks Györgyi and M. Gyulassy for special hospitality at Columbia University. This work has been supported by the HNSF grants OTKA - F4019 and W01015107.

References

[1] Th. Alber et al, NA35 Collaboration: *Phys. Rev. Lett.* **74** (1995) 1303

[2] H. Beker et al, NA44 Collaboration: *Phys. Rev. Lett.* **74** (1995) 3340

[3] T. Alber et al, NA49 Collaboration: *Nucl. Phys.* **A590** (1995) 453c

[4] S. Slegt et al, WA93 Collaboration: *Nucl. Phys.* **A590** (1995) 469c

[5] T. Csörgő, B. Lörstad, J. Zimányi: *Phys. Lett.* **B338** (1994) 134

[6] T. Csörgő: *Phys. Lett.* **B347** (1995) 354

[7] T. Csörgő, B. Lörstad, J. Zimányi: *hep-ph/9411307, Z. Phys. C*, in press

[8] T. Csörgő, B. Lörstad: *hep-ph/9503494, Nucl. Phys.* **A590** (1995) 465c

[9] T. Csörgő, B. Lörstad: *CU-TP-717, LUNFD6/(NFFL-7082)-Rev* (1994), *hep-ph/9509213*

[10] T. Csörgő, B. Lörstad: *Proc. of XXV-th ISMPD*, Stara Lesna, 1995 (World Scientific in press, ed. L. Sandor et al.), *hep-ph/9511404*

[11] Yu. Sinyukov: *Nucl. Phys.* **A566** (1994) 589c

[12] Yu. Sinyukov: in *Proc. HHM:TE* (Divonne, June 1994, Plenum Press, J. Rafelski et al, eds.)

[13] S. V. Akkelin, Yu. M. Sinyukov: *preprint ITP-63-94E*

[14] B.R. Schlei, U. Ornik, M. Plümer, D. Strottman, R.M. Weiner: *preprint LA-UR-95-3232, hep-ph/9509426*

[15] J. Bolz, U. Ornik, M. Plümer, B. R. Schlei, R. M. Weiner: *Phys. Lett.* **B300** (1993) 404

[16] S. Chapman, P. Scotto, U. Heinz: *Phys. Rev. Lett.* **74** (1995) 4400

[17] S. Chapman, P. Scotto and U. Heinz: *hep-ph/9409349, Heavy Ion Physics* **1** (1995) 1;

[18] S. Chapman, J. R. Nix, U. Heinz: *nucl-th/9505032*

[19] U. A. Wiedemann, P. Scotto, U. Heinz: *nucl-th/9508040, Phys. Rev.* **C53** (1996) 918

[20] B. V. Jacak, NA44 Collaboration: *Nucl. Phys.* **A590** () 215c D.E. Fields et al.: *Phys. Rev.* **C52** (1995) 986

[21] T. J. Humanic: *Phys. Rev.* **C50** (1994) 2525

[22] A. Makhlin, Y. Sinyukov: *Z. Phys.* **C39** (1988) 69

[23] S. Pratt, T. Csörgő, J. Zimányi: *Phys. Rev.* **C42** (1990) 2646

[24] W. A. Zajc: in *NATO ASI Series* **B303**, p. 435

[25] S. Chapman, U. Heinz: *Phys. Lett.* **B340** (1994) 250

[26] M. Deutschmann et al: *Nucl. Phys.* **B204** (1982) 333

[27] G. F. Bertsch: *Nucl. Phys.* **A498** (1989) 173c

[28] B. Lörstad: *Int. J. Mod. Phys.* **A12** (1989) 2861

[29] N. Neumeister et al, UA1 Collaboration: *Act. Phys. Slov.* **44** (1994) 113

[30] T. Csörgő, S. Pratt: *KFKI-1991-28/A*, p. 75

[31] F. Cooper, G. Frye: *Phys. Rev.* **D10** (1974) 186

[32] B. Lörstad: hep-ph/9509214